Enhanced ductility and strength in a cast Al-Mg alloy with high Mg content

Zhibo Liu [a], Jiani Sun [a], Zhigang Yan [b], Yaojun Lin [a,*], Manping Liu [c,*], Hans J. Roven [d], Arne K. Dahle [e],

[a] School of Materials Science and Engineering, Wuhan University of Technology, Wuhan, Hubei 430070, China

[b] State Key Laboratory of Metastable Materials Science and Technology, Yanshan University, Qinhuangdao, Hebei 066004, China

[c] School of Materials Science and Engineering, Jiangsu University, Zhenjiang, Jiangsu 212013, China

[d] Department of Materials Science and Engineering, Norwegian University of Science and Technology, 7491 Trondheim, Norway

[e] Department of Materials and Manufacturing, Jönköping University, SE-551 11, Jönköping, Sweden

*Corresponding author: yjlin@whut.edu.cn (Y.J. Lin)
manpingliu@ujs.edu.cn (M.P. Liu)

Abstract

Cast Al-Mg alloys with high Mg content have attracted considerable interest as a result of exceptionally low mass density and enhanced Mg solid-solution strengthening effect. However, poor ductility in this class of cast Al-Mg alloys originating from the increased amount of brittle Al_3Mg_2 phase presents a challenge. This work aims to improve ductility of a cast Al-10wt.%Mg alloy by prolonging time and/or increasing temperature during solid-solution treatment, hence minimizing the amount of the Al_3Mg_2 phase. The amounts of Al_3Mg_2 decrease and the concentrations of solute Mg increase with prolonging time and/or increasing temperature, improving both ductility and strength. Solid-solution treatment at 425 °C for 9 h or at 438 °C for 3 h induces complete dissolution of the Al_3Mg_2 phase, achieving an average uniform elongation of ~27% accompanied by an average 0.2% offset yield strength of ~186 MPa. The mechanisms improving both ductility and strength are discussed.

Keywords: Aluminum alloys; Casting; Ductility; Strength; Solid-solution treatment.

1. Introduction

Cast Al alloys represent a class of Al alloys that are processed by either casting only or casting combined with subsequent heat treatment [1,2]. Simplistic operations and short processing routes for cast Al alloys yield low production costs. Currently, cast Al alloys have been widely used as structural components in aircrafts and ground transportation vehicles due to low production costs and low mass densities, the latter effectively promoting energy conservation and gas emission reduction [1-4]. Among various cast Al alloys, Al-Mg alloys have received particular attention due to lower mass density and better corrosion resistance as compared with those of other cast Al alloys [1,2,5]. Over the past few decades, cast Al-Mg alloys with high Mg contents ranging from 10 to ~40 wt.% have achieved sporadic attention [1,5-13]. The development of cast Al-Mg alloys with high Mg content is stimulated by the

desire to further reduce mass densities [6,14] and simultaneously to improve strength by enhancing the solid-solution strengthening effect of Mg [7,14,15]. Inspection of the published studies [1,7,10], however, indicates that poor ductility in cast Al-Mg alloys with high Mg content poses a challenge for their widespread applications.

Poor ductility may primarily be attributed to the increased amount of brittle Al_3Mg_2 phase stemming from a eutectic reaction (liquid→Al+Al_3Mg_2) during solidification [16]. Although Al-Mg alloys with Mg contents from 10 wt.% to maximum solubility (17 wt.%) do not undergo the eutectic reaction according to the Al-Mg binary equilibrium phase diagram [16], Mg enrichment in remaining liquid phase due to solute partition during the actual solidification process still causes the divorced eutectic reaction [17,18]. In an effort to improve ductility of cast Al-Mg alloys with high Mg content, solid-solution treatment (SST) at the temperatures corresponding to a single-phase solid solution is usually implemented to dissolve the Al_3Mg_2 phase into the Al matrix [1,7,19,20]. For example, after SST at 425 °C (the temperature range of 360-515 °C corresponding to a single-phase solid solution) for 1 h, elongation of the cast Al-10 wt.%Mg alloy can reach 16% with a yield strength (YS) of 180 MPa and ultimate tensile strength (UTS) of 330 MPa, and these data have been well-documented in the literature [1,19]. In order to improve service reliability of the cast Al-10 wt.%Mg alloy, it is desirable to further enhance its ductility. Although a small amount of Al_3Mg_2 phase is still present in Al-10 wt.%Mg alloy solid-solution treated (SST-ed) at 425 °C for 1 h [1,5,19], this alloy content should exhibit a single-phase solid-solution situation in the temperature range of 360-515 °C according to the phase diagram [16]. From this, two questions could be raised. First, is it possible to completely dissolve the Al_3Mg_2 phase by prolonging time and/or increasing temperature during SST, further increasing ductility of the cast Al-10 wt.%Mg alloy? Second, with enhanced solid-solution strengthening by increasing solute Mg concentrations but reduced grain boundary (GB) strengthening due to grain growth, how does SST with prolonged time

and/or increased temperature affect strength of the cast Al-10 wt.%Mg alloy? In view of the aforementioned discussion, the objectives of the present study are two-fold: 1) to explore the feasibility of a complete dissolution of the Al_3Mg_2 phase, maximizing ductility of the cast Al-10wt.%Mg alloy, and 2) to investigate the effect of prolonged time and/or increased temperature during SST on strength of the cast Al-10 wt.%Mg alloy.

2. Experimental

Elements Al and Mg with purity of >99.5 wt.% were used to prepare the Al-10 wt.%Mg alloy. The weighted elements Al and Mg were melted by induction heating and the Al-10wt.%Mg alloy was cast into a non-preheated cylindrical steel mold with inner diameter of 60 mm and length of 240 mm without the addition of inoculants. The composition of the as-cast alloy was determined via chemical analysis as follows (wt.%): Mg 9.75, Fe 0.05, Si 0.22, Zn 0.04, Cu 0.02 and Al balance. In order to study the effects of prolonging time and increasing temperature during SST on dissolution of Al_3Mg_2 phase, the documented solid-solution processing parameters of cast Al-10 wt.%Mg alloy in Ref. 1, i.e., 425 °C for 1 h, were taken as a baseline. In the study of the effect of prolonging time, the same solid-solution temperature as that in Ref. 1, i.e., 425 °C, was selected, and the as-cast materials sectioned from the ingots were SST-ed at 425 °C for 1, 3 and 9 h, followed by quenching into 40 °C water. To investigate the effect of increasing temperature, the solid-solution temperature was chosen to be higher than 425 °C but lower than the eutectic temperature of 450 °C, given Mg inter-dendritic segregation that results in melting in some local regions of the as-cast Al-10wt.%Mg alloy at the solid-solution temperatures above 450 °C. To avoid the melting risk, in the present study the increased solid-solution temperature was arbitrarily selected as the halfway temperature, i.e., 438 °C, between 425 °C and 450 °C, and the as-cast materials taken from the ingots were SST-ed at 438 °C for 1 and 3 h, and then also quenched by 40 °C water. The Al_3Mg_2 phase in

the as-cast alloy was identified using energy dispersive spectrometry (EDS) equipped with a FEI Quanta FEG 250 scanning electron microscopy (SEM) operated at 20 kV. The Al_3Mg_2 phase in the as-cast and SST-ed alloys were also examined using secondary electron imaging (SEI) obtained with the above FEI Quanta FEG 250 SEM operated at 20 kV. Grain sizes in those SST-ed alloys were studied using a Leica DM2500 M optical microscopy (OM) under polarized light. Since dendrites can also be revealed by polarized light, rendering it difficult to correctly recognize grain contours, the grain size in the as-cast alloy was investigated using electron backscatter diffraction (EBSD) in the aforementioned FEI Quanta FEG 250 SEM equipped with an Oxford EBSD detector. EBSD analysis was conducted under the following parameters: acceleration voltage 20 kV, working distance 15 mm, tilt 70°, and scanning step 6 μm. EBSD data were processed using the HKL channel 5 OIM software. X-ray diffraction (XRD) analysis was also performed on the as-cast and SST-ed alloys in a Bruker D8 Advance diffractometer using Cu Kα radiation with scanning rate of 0.4° per minute. Tensile tests were conducted at room temperature under an initial strain rate of 5×10^{-4} s^{-1} using an Instron-5966 Tester equipped with a video extensometer. During tensile tests, the strains in the gauge sections were accurately measured by the video extensometer. Herein dog-bone shaped specimens with a gauge length of 10 mm and a cross-section of 2.5 mm × 0.5 mm were used. For the consistence of measured results, more than three specimens were tested for each type of as-cast and SST-ed alloys. After tensile tests, fracture surfaces were observed using SEI obtained with the preceding FEI Quanta FEG 250 SEM operated at 20 kV.

3. Results

Fig. 1 shows the SEM microstructures of the Al-10 wt.%Mg alloys as-cast and SST-ed. Careful inspection of a series of SEM SEI micrographs of the as-cast and SST-ed Al-10wt.%Mg alloys reveals porosity of approximately 0.5-0.8% in volume fraction with pore sizes smaller

than approximately 2-4 μm. The as-cast Al-10wt.%Mg alloy contains a high volume fraction of inter-dendritic second-phase particles, most of which exhibit curved-plate geometry as pointed by the arrows in Fig. $1a_1$. As shown in Fig. $1a_2$, the typical result of EDS quantitative analysis on the second-phase particles in Fig. $1a_1$ indicates that the particles include only Al and Mg with approximately 3:2 of the ratio of Al to Mg atomic percentages. Thus, the second-phase could be identified as Al_3Mg_2. As shown in Fig. $1a_3$, statistical analysis of randomly selected Al_3Mg_2 particles in a series of SEM SEI micrographs indicates that the intercepted lengths of the curved-plate shaped Al_3Mg_2 particles in the observed plane, which critically affect stress concentration and cracking, fall in the range of ~5 - ~260 μm with average intercepted length of ~35 μm in the as-cast Al-10 wt.%Mg alloy. After SST at 425 °C for 1 h, the volume fraction of the Al_3Mg_2 phase decreases significantly as a result of dissolution; however, a small amount of Al_3Mg_2 phase is still present, as shown in Fig. $1b_1$. Statistical analysis of randomly selected remaining Al_3Mg_2 particles shows the range of intercepted lengths of Al_3Mg_2 particles of ~4 - ~120 μm with average intercepted length of ~20 μm (see Fig. $1b_2$). By prolonging the solution time to 3 h or increasing temperature to 438 °C, the Al_3Mg_2 phase almost disappears; however, a few Al_3Mg_2 particles having intercepted lengths of ~2 - ~32 μm with average intercepted length of ~16 μm and intercepted lengths of ~2 - ~29 μm with average intercepted length of ~11 μm are occasionally observed, as displayed in Figs. 1c and e, respectively. With further prolonging time to 9 h at 425 °C or 3 h at 438 °C, no Al_3Mg_2 phase can be observed, as demonstrated in Figs. 1d and f.

Fig. 2 demonstrates the XRD patterns of the as-cast and SST-ed Al-10 wt.%Mg alloys. The peaks of the Al_3Mg_2 phase can be clearly seen for the as-cast alloy. The peak intensity significantly decreases after SST at 425 °C for 1 h. With prolonging time (425°C for 3 and 9 h) and/or increasing temperature (438°C for 1 and 3 h), the peaks of the Al_3Mg_2 phase essentially cannot be detected. These XRD results are consistent with EDS identification and SEM

observations. The lattice constants of the Al matrices in the as-cast and SST-ed alloys can be determined from the XRD results by fitting based on the Nelson-Riley function [21], as reported in Table 1. The corresponding solute Mg concentrations can be estimated on the basis of an increase by 0.0046 Å per 1 at.% of solute Mg [22] with lattice constant 4.0495 Å being the baseline for pure Al [23] (see Table 1).

The EBSD map in Fig. $3a_1$ and the OM micrographs in Figs. $3b_1$ through f_1 display equiaxed grains in the as-cast and SST-ed conditions. The corresponding statistical distributions of grain sizes, together with average grain sizes, $\bar{d}$, evaluated by fitting with a lognormal probability function [24,25], are presented in Figs. $3a_2$ through f_2. Comparison of the average grain size in the as-cast alloy, $\bar{d}$=93 μm, with those in the SST-ed conditions suggests that grain growth occurs during SST.

Fig. 4a shows typical tensile engineering stress-strain curves of the as-cast and SST-ed Al-10 wt.%Mg alloys. To better highlight the 0.2% offset YS, the section enclosed by a dashed rectangle in Fig. 4a is enlarged, as shown in Fig. 4b. Fig. 4c displays tensile true stress (σ)-strain (ε) curves converted from the corresponding engineering curves in Fig. 4a using the standard formula. To accurately locate uniform elongation, the work hardening rate curves ($d\sigma/d\varepsilon$ vs. ε) are superimposed to the true stress-strain curves as shown in Fig. 4d. Here the true strain at $d\sigma/d\varepsilon=\sigma$ corresponds to the uniform elongation in terms of the considère criterion [26]. The true strains at $d\sigma/d\varepsilon=\sigma$ are labeled in Fig. 4c using squares, and the determined uniform elongations are marked in Fig. 4a using circles. Furthermore, the statistical tensile properties of the as-cast and SST-ed conditions acquired from more than three specimens are presented in Table 2. The slightly different tensile properties for each type of as-cast and SST-ed alloys are likely attributed to slightly different levels of casting defects, e.g., pores, microcracks, etc. By SST, both strength and ductility are improved as compared with those of the as-cast alloy and moreover, both strength and ductility increase with either prolonging time

or increasing temperature during SST. Noteworthy is that, by SST at 425 °C for 9 h and at 438 °C for 3 h, the Al-10 wt.%Mg alloy can achieve uniform elongations of 27.1% and 26.6%, YS of 185 MPa and 186 MPa, engineering UTS of 387 MPa and 385 MPa, and true UTS of 492 MPa and 487 MPa, respectively. In addition, as shown in Figs. 4a, c and d, the work-hardening rates of the SST-ed alloys are higher than that of the as-cast alloy, and the work-hardening rates are improved with prolonging time or/and increasing temperature during SST, as a result of increased solute Mg concentrations [27,28].

Fig. 5 displays the fracture surfaces of the as-cast and SST-ed Al-10 wt.%Mg alloy after tensile testing. The fracture surface of the as-cast alloy consists of most matrix/Al_3Mg_2 phase interfaces and a small amount of morphology featured by small and shallow dimples (Fig. 5a). After SST at 425 °C for 1 h, the fracture surface comprises most dimples and few matrix/Al_3Mg_2 phase interfaces (Fig. 5b). With prolonging time (425 °C for 3 h) or increasing temperature (438 °C for 1 h), the fracture surfaces as shown in Figs. 5c and e are characterized by entire dimples larger and deeper than those corresponding to SST at 425 °C for 1 h (Fig. 5b). With further prolonging time (425 °C for 9 h) and/or increasing temperature (438 °C for 3 h), as shown in Figs. 5d and f , the fracture surfaces are still featured by entire dimples that become further larger and deeper relative to those in Figs. 5c and e.

4. Discussion

The presence of brittle Al_3Mg_2 phase with size on the order of a few to a few hundreds micrometers induces stress concentrations and promotes the occurrence of strain localization, necking and final tensile fracture. In the as-cast alloy, a high volume fraction of Al_3Mg_2 phase induces extensive stress concentrations and consequently, strain localization and fracture set in immediately after yielding, leading to very low ductility (uniform elongation of 0.6%). This is consistent with the fracture surface consisting of most matrix/Al_3Mg_2 phase interfaces and few

small and shallow dimples (Fig. 5a), the latter providing the limited ductility. By SST at 425 °C for 1 h, only a small amount of Al_3Mg_2 phase is retained and hence the stress concentration level is significantly reduced. As a result, strain localization is delayed until an appreciable strain magnitude is reached (engineering strain of 16.1%), and this is accompanied by a fracture surface comprising larger and deeper dimples and occasional matrix/Al_3Mg_2 phase interfaces (Fig. 5b). With prolonging time (425 °C for 3 h) or increasing temperature (438 °C for 1 h), only few Al_3Mg_2 particles are present and the onset of strain localization is further postponed to higher strain levels (engineering strains of 20.9% and 23.9%, respectively). The fracture surfaces have accordingly large quantities of dimples (Figs. 5c and e). With further prolonging times (425 °C for 9 h and 438 °C for 3 h), no Al_3Mg_2 phase is evident and stress concentration from the Al_3Mg_2 phase is thus minimized. Accordingly, uniform elongations can reach maximum values (engineering strains of 27.1% and 26.6%). Corresponding fracture surfaces are featured by dimples (Figs. 5d and f) being even larger and deeper than those seen for 425 °C for 3 h (Fig. 5c) and 438 °C for 1 h (Fig. 5e).

In terms of porosity of approximately 0.5-0.8% in volume fraction and pore sizes smaller than approximately 2-4 μm in the as-cast and SST-ed Al-10wt.%Mg alloys as presented in Section 3 “Results”, pores should insignificantly affect the mechanical properties. Given the interspacing between Al_3Mg_2 particles on the order of a few tens to hundreds micrometers (Fig. 1) and a relatively low density of dislocations in the as-cast and SST-ed alloys [1,5], particle and dislocation strengthening can be neglected. Hence, the primary strengthening mechanisms in the present case involve Mg solid-solution and GB strengthening. The increment in YS contributed by GB strengthening, $\Delta\sigma_{y,g}$, can be evaluated using the Hall-Petch relation: $\Delta\sigma_{y,g} = kd^{-1/2}$, where k is the Hall-Petch slope taken as 105 MPa $\mu m^{1/2}$ for Al-Mg alloys [29]. The increment in YS contributed by Mg solid-solution strengthening, $\Delta\sigma_{y,s}$, is estimated based on the increased value in YS by solid-solution strengthening of 1 at.% Mg, i.e., 17.2 MPa [1].

Taking the increments in YS contributed by GB and Mg solid-solution strengthening in the as-cast Al-10 wt.%Mg alloy as the references, the corresponding values in the SST-ed conditions are evaluated and presented in Table 3. With prolonging time and/or increasing temperature, increments in YS contributed by GB strengthening decrease due to grain growth, whereas those contributed by Mg solid-solution strengthening increase due to increased solute Mg concentrations as a result of dissolution of the Al_3Mg_2 phase. However, due to grain sizes as large as 93-156 μm, the decreases in increments by GB strengthening are insignificant with increasing grain sizes. Consequently, the increase in increments by Mg solid-solution strengthening can surpass the decreases in increments by GB strengthening, leading to an overall increase in YS with prolonging time and/or increasing temperature during SST. The calculated overall increments of YS reported in Table 3 are in reasonably good agreement with the experimental values shown in Table 2. With prolonging time and/or increasing temperature, both work-hardening rate and uniform elongation increase, enabling the occurrence of more work hardening in the stage of uniform elongation during tensile testing, which, together with the increased YS, yields increased UTS.

5. Conclusions

Prolonging time or/and increasing temperature during SST can improve both ductility and strength of the cast Al-10 wt.%Mg alloy. The increase in ductility stems from a decrease in the amount of Al_3Mg_2 phase, reducing stress concentration at the Al matrix/Al_3Mg_2 phase interfaces and hence delaying the occurrence of strain localization, necking and fracture. The increase in YS can be attributed to enhanced Mg solid-solution strengthening originating from dissolution of the Al_3Mg_2 phase, which more than compensates for decreased GB strengthening due to grain growth. The combination of increased yield strength, work-hardening rates and uniform elongations facilitates increased UTS values. SST at 425 °C for 9 h or at 438 °C for 3

h induces complete dissolution of the Al_3Mg_2 phase. The present high Mg containing Al-Mg alloys therefore achieves an average uniform elongation of 26.6-27.1%, accompanied by an average YS of 185-186 MPa, average engineering UTS of 385-387 MPa, and average true UTS of 487-492 MPa.

Acknowledgements

The present study was financially supported by the National Natural Science Foundation of China (Grant numbers: U1810108 and U1710124).

References

[1] J.R. Davis, Aluminum and Aluminum Alloys, ASM International, Materials Park, OH, 1993.

[2] R. Lumley, Fundamentals of Aluminium Metallurgy: Production, Processing and Applications, 1st ed., Woodhead Publishing, 2011.

[3] J.C. Williams, E.A. Starke Jr, Acta Mater. 51(2003)5775-5799.

[4] W.S. Miller, L. Zhuang, J. Bottema, A.J. Wittebrood, P. De Smet, A. Haszler, A. Vieregge, Mater. Sci. Eng. A 280(2000)37-49.

[5] M. Glazoff, A. Khvan, V. Zolotorevsky, N. Belov, A. Dinsdale, Casting Aluminum Alloys: Their Physical and Mechanical Metallurgy, 2nd ed., Butterworth-Heinemann, 2019.

[6] S. Scudino, M. Sakaliyska, K.B. Surreddi, F. Ali, J. Eckert, J. Alloys Compd. 504S(2010)S483-S486.

[7] Y. Harada, N. Jiang, S. Kumai, Mater. Trans. 60(2019)2435-2441.

[8] J.R.P. Rodrigues, M. de Lourdes Noronha Motta Melo, R.G. dos Santos, J. Mater. Sci. 45(2010)2285-2295.

[9] H.W. Kim, C.Y. Lim, S.B. Kang, Adv. Mater. Res. 29-30(2007)83-86.

[10] Y. Kojima, T. Takahashi, M. Kubo, T. Morinaga, Metall. Trans. A 12(1981)1113-1117.

[11] D. Hamana, M. Bouchear, M. Betrouche, A. Derafa, N.Y. Rokhmanov, J. Alloys Compd. 320(2001)93-102.

[12] J.C. Jie, C.M. Zou, H.W. Wang, B. Li, Z.J. Wei, Scr. Mater. 64(2011)588-591.

[13] J.C. Jie, C.M. Zou, E. Brosh, H.W. Wang, Z.J. Wei, T.J. Li, J. Alloys Compd. 578(2013)394-404.

[14] D.H. Jang, Y.B. Park, W.J. Kim, Mater. Sci. Eng. A 744(2019)36-44.

[15] B.H. Lee, S.H. Kim, J.H. Park, H.W. Kim, J.C. Lee, Mater. Sci. Eng. A 657(2016)115-122.

[16] H. Okamoto, L. Kacprzak, P. Subramanian, Binary Alloy Phase Diagrams, ASM International, Materials Park, OH, 1996.

[17] W. Kurz, D.J. Fisher, Fundamentals of Solidification, 4th ed., Trans Tech Publications Ltd, Zurich, Switzerland, 1998.

[18] G.K. Sigworth, Int. J. Metalcast. 8(1)(2014)7-20.

[19] J.G. Kaufmann, E.L. Rooy, Aluminum Alloy Castings: Properties, Processes, and Applications, ASM International, Materials Park, OH, 2004.

[20] M.J. Starink, A.M. Zahra, Acta Mater. 46(1998)3381-3397.

[21] B.D. Cullity, S.R. Stock, Elements of X-ray Diffraction, 3rd ed., Prentice-Hall, Upper Saddle River, NJ, 2001.

[22] J.E. Hatch (ed.), Aluminum Properties and Physical Metallurgy, ASM International, Materials Park, OH, 1984.

[23] W.J. Helfrich, R.A. Dodd, Trans. AIME 224(1962)757-762.

[24] Y.H. Zhao, X.Z. Liao, Z. Jin, R.Z. Valiev, Y.T. Zhu, Acta Mater. 52(2004)4589–4599.

[25] S. Zhang, W. Hu, R. Berghammer, G. Gottstein, Acta Mater. 58(2010)6695–6705.

[26] G.E. Dieter, Mechanical Metallurgy, 3rd ed., McGraw-Hill, New York, 1986.

[27] M. Zha, Y. Li, R.H. Mathiesen, R. Bjørge, H.J. Roven, Acta Mater. 84(2015)42-54.

[28] T.H. Courtney, Mechanical Properties of Materials, Waveland Press, Long Grove, IL, USA,

2005.

[29] M. Furukawa, Z. Horita, M. Nemoto, R.Z. Valiev, T.G. Langdon, Acta Mater. 44(1996)4619-4629.

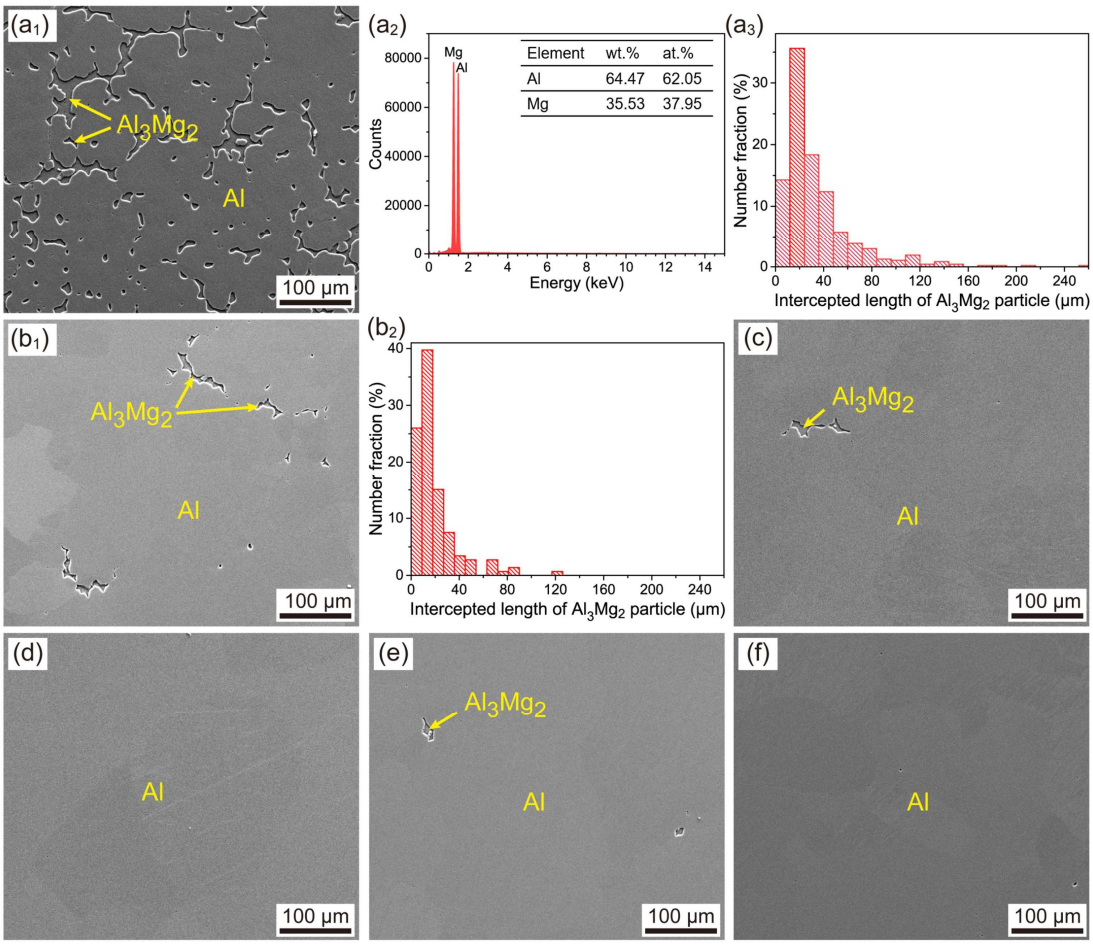

Fig. 1. SEM SEI micrograph (a_1), the typical result of EDS quantitative analysis on Al_3Mg_2 particles (a_2) and statistical distribution of intercepted lengths of curved-plate shaped Al_3Mg_2 particles in the observed plane (a_3) in the as-cast Al-10wt.%Mg alloy, SEM SEI micrograph (b_1) and statistical distribution of intercepted lengths of curved-plate shaped Al_3Mg_2 particles in the observed plane (b_2) in the Al-10wt.%Mg alloy SST-ed at 425 °C for 1 h, and SEM SEI micrographs in the Al-10wt.%Mg alloys SST-ed at 425 °C for 3 h (c) and 9 h (d) and at 438 °C for 1 h (e) and 3 h (f), respectively.

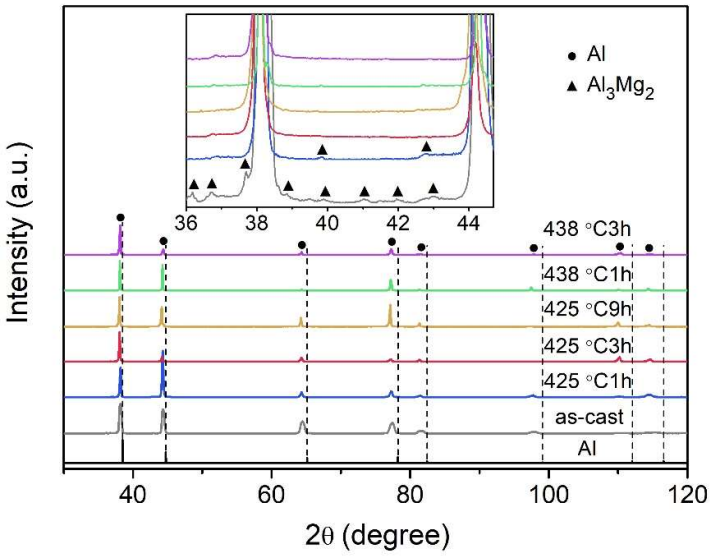

Fig. 2. XRD patterns of the as-cast and SST-ed Al-10 wt.%Mg alloys.

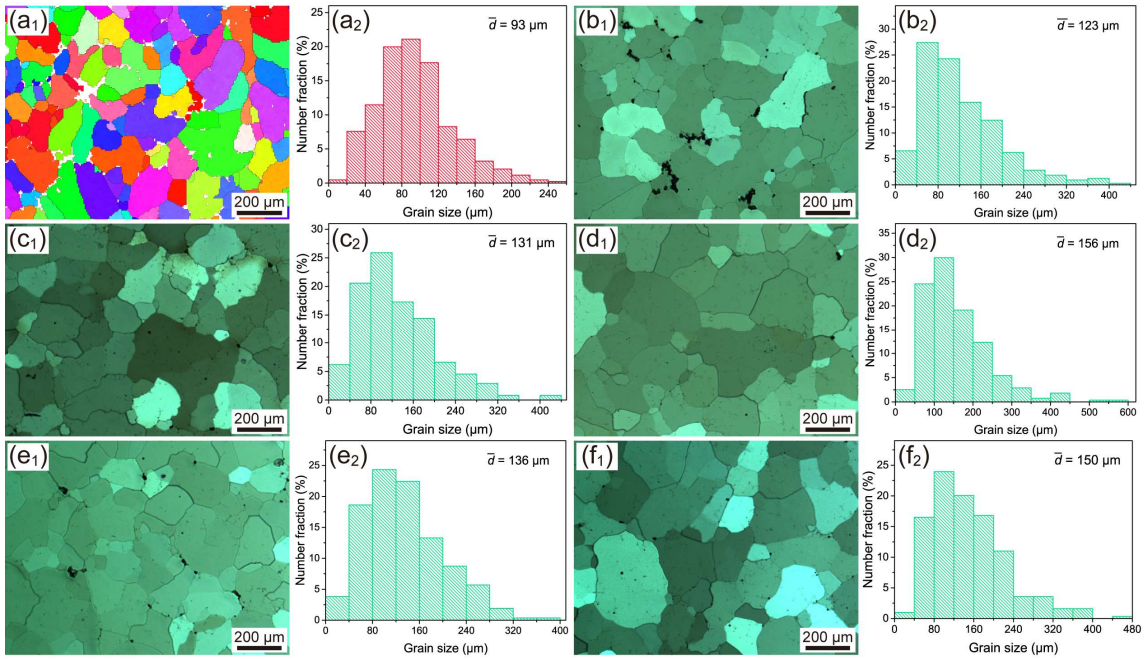

Fig. 3. Grain morphologies and sizes of the Al-10 wt.%Mg alloys as-cast (a_1) and SST-ed at 425 °C for 1 h (b_1), 3 h (c_1), and 9 h (d_1), and at 438 °C for 1 h (e_1) and 3 h (f_1), together with statistical distributions of grain sizes (a_2-f_2) corresponding to (a_1-f_1), respectively.

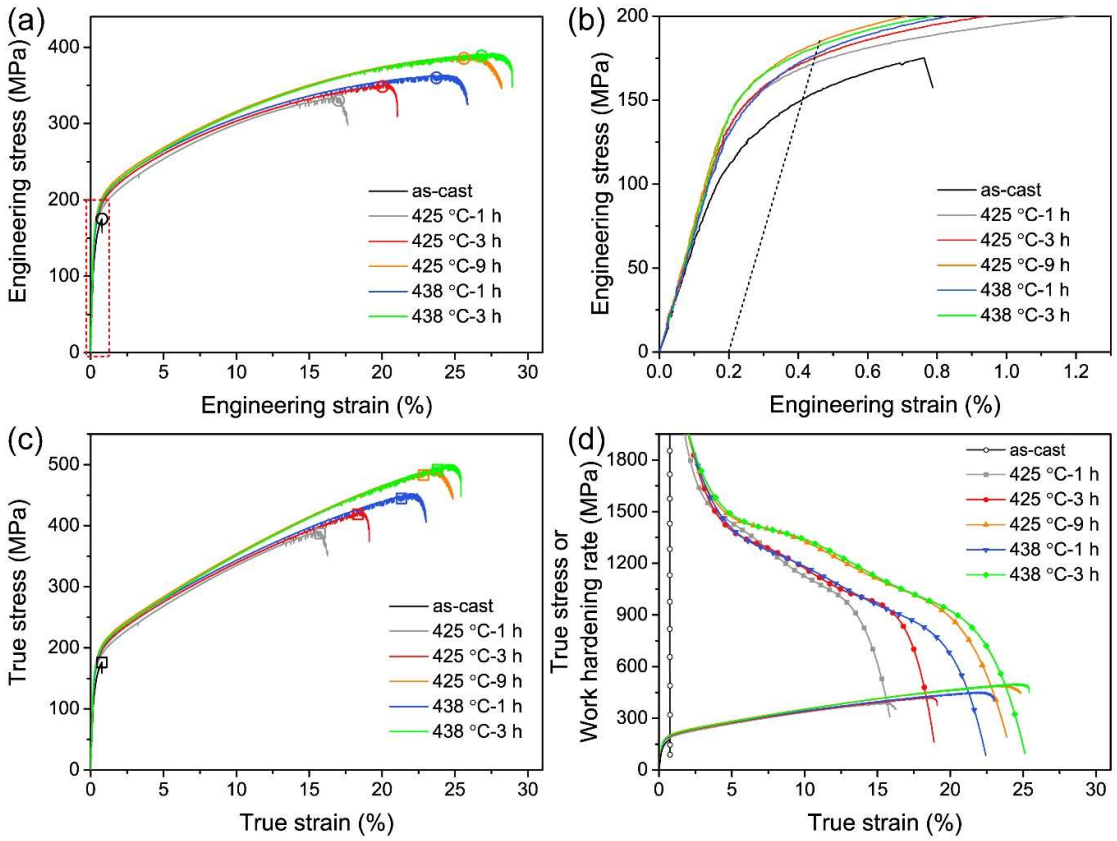

Fig. 4. Tensile properties of the as-cast and SST-ed Al-10wt.%Mg alloys: (a) engineering stress-strain curves, (b) the enlarged section enclosed by the dashed rectangle in (a), (c) true stress-strain (σ-ε) curves, and (d) work hardening rate (dσ/dε) curves superimposed by true stress-strain curves.

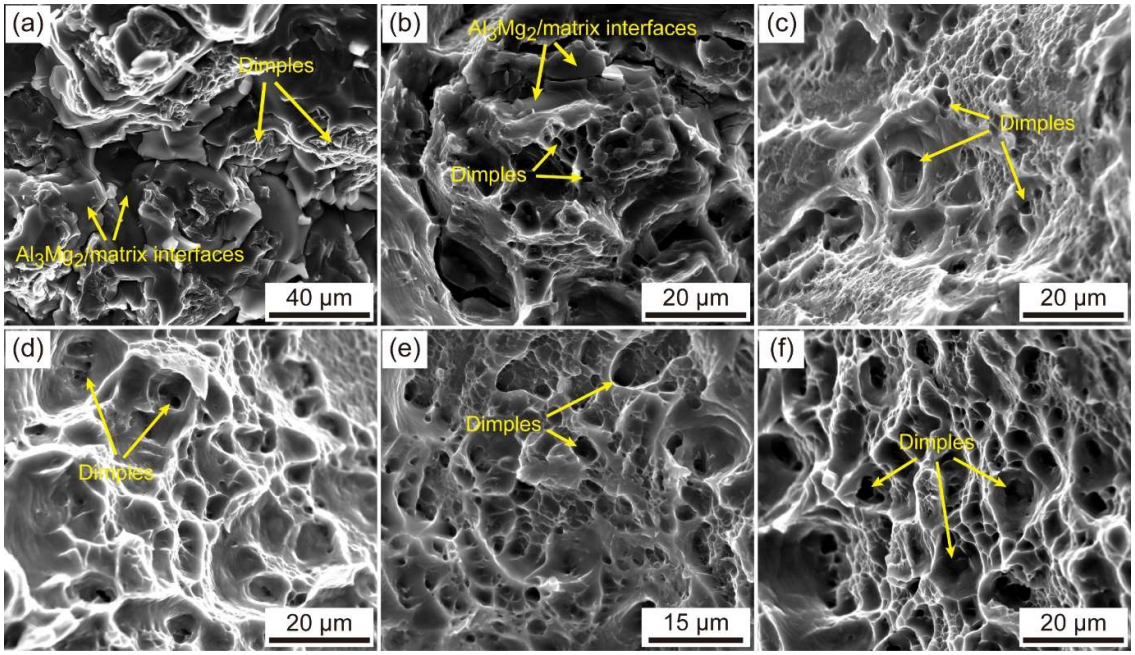

Fig. 5. SEM SEI micrographs of fracture surfaces of the as-cast (a) and SST-ed Al-10 wt.%Mg alloys at 425 °C for 1 h (b), 3 h (c), and 9 h (d), and at 438 °C for 1 h (e) and 3 h (f).

Table 1

Lattice constants and solute Mg concentrations in the as-cast and SST-ed Al-10 wt.%Mg alloys.

Status	Lattice constant (Å)	Solute Mg concentration (at.%)	Solute Mg concentration (wt.%)
As-cast	4.0867	8.09	7.34
Solid-solution treated			
425 °C-1 h	4.0949	9.86	8.97
425 °C-3 h	4.0967	10.26	9.34
425 °C-9 h	4.0987	10.70	9.74
438 °C-1 h	4.0973	10.39	9.46
438 °C-3 h	4.0986	10.67	9.71

Table 2

Tensile properties of the as-cast and SST-ed Al-10 wt.%Mg alloys.

Status	YS (MPa)	UTS (MPa)		Uniform elongation (%)	True strain at $d\sigma/d\varepsilon=\sigma$ (%)
		Engineering	True		
As-cast	150 ± 1	164 ± 11	165 ± 11	0.6 ± 0.2	0.6 ± 0.2
Solid-solution treated					
425 °C-1 h	172 ± 2	330 ± 8	383 ± 9	16.1 ± 2.5	14.9 ± 2.2
425 °C-3 h	175 ± 1	358 ± 9	433 ± 11	20.9 ± 1.7	19.0 ± 1.4
425 °C-9 h	185 ± 3	387 ± 3	492 ± 4	27.1 ± 2.0	24.0 ± 1.6
438 °C-1 h	177 ± 1	362 ± 3	449± 4	23.9 ± 0.7	21.4 ± 0.6
438 °C-3 h	186 ± 3	385 ± 3	487 ± 4	26.6 ± 1.5	23.6 ± 1.2

Table 3

Increments in YS of the SST-ed Al-10 wt.%Mg alloys contributed by GB strengthening and Mg solid-solution strengthening with those in the as-cast condition used as references (MPa)

Material	GB strengthening (MPa)	Mg solid-solution strengthening (MPa)	Total (MPa)
As-cast	0	0	0
Solid-solution treated			
425 °C-1 h	-1.4	+30.4	+29.0
425 °C-3 h	-1.7	+37.3	+35.6
425 °C-9 h	-2.5	+44.9	+42.4
438 °C-1 h	-1.9	+39.6	+37.7
438 °C-3 h	-2.3	+44.4	+42.1